https://doi.org/10.3311/PPch.37544

Periodica Polytechnica Chemical Engineering, 68(4), pp. 665–679, 2024

Comparative Performance Analysis of Catalysts for Syngas Production from Biogas: A Simulation Study Using DWSIM

Afdal Adha[1*], Arie Rahmadi[1]

[1] Research Center for Process and Manufacturing Industry Technology, National Research and Innovation Agency (BRIN), Gedung B.J. Habibie, Jl. M.H. Thamrin 8., 10340 Jakarta, Indonesia
[*] Corresponding author, e-mail: afda002@brin.go.id

Received: 29 May 2024, Accepted: 01 October 2024, Published online: 21 October 2024

Abstract

This study explored how CH_4/CO_2 feed ratio, temperature, and pressure affect the conversion of carbon dioxide and methane and the H_2/CO ratio of syngas using simulations for six catalysts: Rh/La_2O_3, Rh/La_2O_3-SiO_2, Ru/La_2O_3, Ni-Co/Al-Mg-O, $LaNiO_3$, and Ce-La-Ni-O_2. Simulations with DWSIM© were conducted at CH_4/CO_2 feed ratios of 1–2, pressures of 1–5 bar, and temperatures of 550–750 °C. The effects showed that increasing the temperature by as much as 750 °C boosted the H_2/CO ratio and improved CO_2 and CH_4 conversions because of the endothermic nature of the reactions. Higher pressure reduced conversion rates and H_2/CO ratios across all catalysts, with a notable similarity between 2 and 5 bar, indicating thermodynamic limits. A higher feed ratio of CH_4/CO_2 decreased CH_4 conversion while increasing the H_2/CO ratio at the expense of reduced H_2 yield. As the pressure decreases, the Ru/La_2O_3 and Rh/La_2O_3-SiO_2 catalysts exhibited higher activity because of the kinetic factor. The current research focuses on the possibility of using dry reforming of biogas to synthesize syngas with suitable H_2/CO ratios for different uses. The observations suggest that future studies should include techno-economic analysis to determine the least expensive catalysts that will ensure the dry reforming process yields the right composition of syngas.

Keywords

biogas dry reforming, catalyst performance, DWSIM simulation, H_2/CO ratio, syngas production

1 Introduction

A mixture of CO and H_2, syngas, can be further used in other production including methanol, liquid fuels, and diverse chemicals making it a valuable intermediate for manufacturing high-value industrial products as well. Syngas can be provided from every oil source such as natural gas, coal, biomass, biogas, and organic wastes. Biogas, as a renewable gas, is a promising input for syngas formation [1–4]. Biogas is a clean gaseous fuel when it is produced and combusted [5, 6].

Biogas is the main product of anaerobic digestion, a mixture of gases primarily composed of CH_4 and CO_2 with various quantities of contaminants, such as hydrogen sulfide, nitrogen, water vapor, ammonia, oxygen, methyl siloxanes, carbon monoxide, halogenated volatile organic compounds (VOCs) and hydrocarbons, while the by-product is digestate, a nutrient-rich residual material that can be used as fertilizer [7–10]. Before further use, biogas needs to be treated to eliminate any toxic constituents. Biogas treatment has two steps: cleaning and upgrading, as shown in Fig. 1(a). Cleaning removes unwanted and toxic substances like H_2S, NH_3, O_2, N_2, Si, H, CO, and VOCs. Upgrading changes the CO_2 concentration to make the calorific value of the biogas better [10]. In direct use for syngas production through dry reforming of methane (DRM), the biogas upgrading stage is not necessary, so there are no additional costs associated with this process. Clean model biogas with high CO_2 levels (30–45% or above) and CH_4 (55–75% or below) is good for DRM as direct conversion into syngas. In a renewable biomass-to-syngas conversion process using DRM, biogas serves as an intermediar that may be utilized in power generating applications or used to make valuable chemicals (such as methanol) and liquid fuels via the Fischer-Tropsch synthesis [11, 12].

The DRM to syngas process is gaining popularity from an environmental and an industrial standpoint. The DRM reaction has been regarded as a great scheme and a good alternative for combining these two things; it produces syngas while significantly reducing global warming by

Cite this article as: Adha, A., Rahmadi, A. "Comparative Performance Analysis of Catalysts for Syngas Production from Biogas: A Simulation Study Using DWSIM", Periodica Polytechnica Chemical Engineering, 68(4), pp. 665–679, 2024. https://doi.org/10.3311/PPch.37544

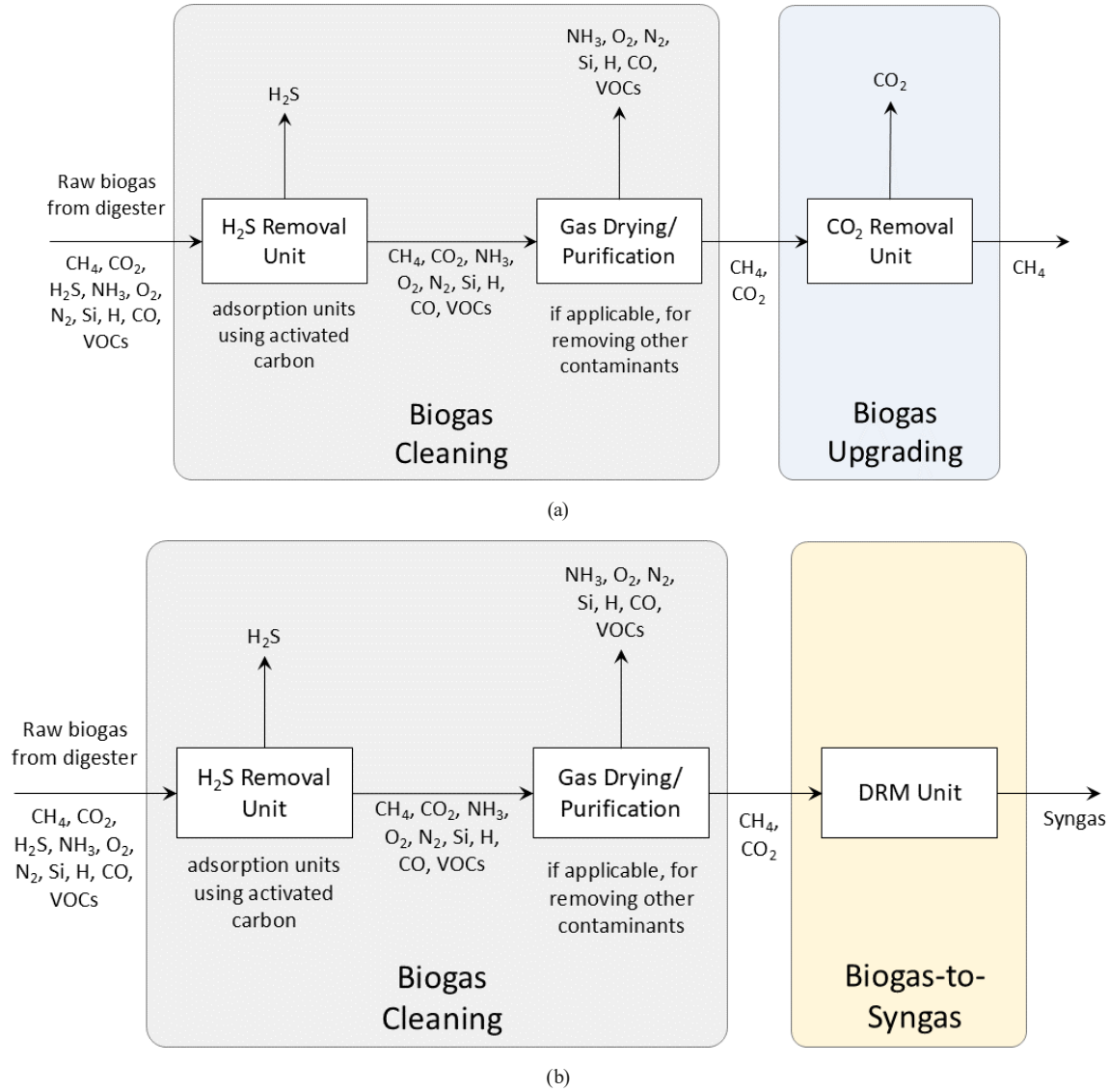

Fig. 1 Block flow diagram (BFD): (a) Biogas treatment; (b) Biogas-to-Syngas through DRM

simultaneously utilizing both of the major greenhouse gases (CO_2 and CH_4). The syngas generated through the DRM process have a low ratio of H_2/CO (nearly 1). It is immediately applicable as an input material for the production of organic molecules containing oxygen: methanol and acetic acid. In addition, it can be employed in the Fischer-Tropsch synthesis method to generate hydrocarbons with a long chain [8, 13, 14]. The DRM reaction, Eq. (1), produces a 1:1 H_2/CO ratio. In contrast, the concurrent reverse water-gas shift (RWGS) reaction, Eq. (2), results in an H_2/CO ratio that is smaller than 1 [8, 15–19].

$$CH_4 + CO_2 \leftrightarrow 2CO + 2H_2, \ \Delta H^{\circ}_{25\,^{\circ}C} = 247 \ \text{kJ mol}^{-1} \quad (1)$$

$$CO_2 + H_2 \leftrightarrow CO + H_2O, \ \Delta H^{\circ}_{25\,^{\circ}C} = 41 \ \text{kJ mol}^{-1} \quad (2)$$

Equation (1) thus displays that the DRM process has a strong endothermic nature and requires the addition of heat. In these circumstances, the catalyst service life is significantly shortened because of sintering and/or coke deposition. Recently, significant research efforts have focused on developing catalysts that not only excel in syngas production but also demonstrate enhanced resistance to coking and sintering, ensuring their durability and long-term performance [14]. The application of several metal catalysts supported on various materials in the DRM process has been investigated. Lanthanum-based supports for catalyst from noble metal, like Rh and Ru [20–22], non-noble catalysts such as nickel [23–25] metal-oxide-supported nickel catalysts [4, 7, 11–13, 26] have demonstrated encouraging selectivity and activity for syngas production. These catalysts show high catalytic performance along with effective properties for reducing coke formation.

DWSIM© [27] is an open-source chemical engineering simulator with easy access, a powerful thermodynamic

package, and an interactive graphical interface for component performance analysis. DWSIM provides mass and energy balances at a steady state, besides giving some of the most advanced models and processes for data analysis. It is reliable, easy to interpret, and has a high convergence rate compared to other simulation tools [28, 29].

Previous studies have utilized DWSIM to analyze and simulate the operation of combined cycle and gas turbine (CCGT) power plants under normal conditions. DWSIM simulations of CCGT plants are highly reliable for operator training, academic research, and process optimization under design conditions [29]. A comparative study between Aspen Plus and DWSIM for booster and sales gas compression is presented by Tangsriwong et al. [30]. It has been shown that DWSIM can simulate the chemical processes properly and calculate the thermodynamics and chemical properties, especially for gas products. Andreasen [31] provides an in-depth review of DWSIM. The outcomes obtained from DWSIM simulation software are contrasted with those from a widely utilized commercial process simulator in the industry using a previously reported oil and gas separation plant simulation model. The compared results show a maximum deviation of 1%. These positive results demonstrate the validity of using free and open-source simulation software professionally.

To the best of our knowledge, no previous study has compared various catalysts in the simulation of biogas reforming or DRM using DWSIM. Nonetheless, Zhao et al. [32] performed simulations by combining DRM and steam reforming of methane (SRM) using Visual Basic TM. The study compared two Ni-based catalysts (from Park et al. [33] and Zhang et al. [26]) in a conventional downfired reformer. The simulation findings indicate that the catalyst proposed by Zhang et al. [26] exhibits greater activity compared to the catalyst suggested by Park et al. [33] for the DRM reaction.

The aim of this study is to simulate syngas production from biogas using different catalysts, evaluating the operating conditions effects on catalyst performance. Key performance metrics include the ratio of H_2/CO in the syngas products and CH_4 and CO_2 conversion rates. This analysis will leverage the DWSIM simulation tool to identify optimal catalysts and conditions for efficient syngas production, contributing to advancements in sustainable hydrogen production and greenhouse gas utilization.

2 Kinetic rate models

There have been numerous studies in the literature regarding catalyst development for biogas reforming (DRM reaction). However, only a limited number have investigated the catalytic reaction mechanism and derived the kinetic rate model and its parameters. In the literature, we found several researchers who designed catalysts together with kinetic rate models and parameters.

2.1 Kinetic rate model of Rh/La_2O_3 catalyst

Using their Rh/La_2O_3 catalyst, Múnera et al. [20] investigated the DRM reaction kinetically at atmospheric pressure (550–630 °C) with different CO_2/CH_4 ratios. CH_4 adsorbs on Rh clusters and cracks to produce H_2, while La_2O_3 promotes oxycarbonate species formation from CO_2. CO is generated slowly from surface carbon at the metal or oxide-metal interface. The kinetic rate model is presented in Eq. (3). The proposed kinetic equation fits experimental data well. Table 1 [20–22, 24–26, 34–36] provides the temperature dependencies of the kinetic parameters (the list of parameter symbols is given in Nomenclature at the end of the article).

$$r_{CH_4} = \frac{K_1\, k_2\, k_3\, p_{CH_4}\, p_{CO_2}}{K_1\, k_3\, p_{CH_4}\, p_{CO_2} + K_1\, k_2\, p_{CH_4} + k_3\, p_{CO_2}} \tag{3}$$

2.2 Kinetic rate model of Rh/La_2O_3-SiO_2 catalyst

Expanding on their prior research, Múnera et al. [21] conducted kinetic investigation of the DRM reaction over Rh/La_2O_3-SiO_2 catalyst under ambient conditions (550–630 °C) and with varying CO_2/CH_4 ratios. The detected mechanism of the reaction was identical to that described in [20] for the Rh/La_2O_3 catalyst. The kinetic rate model is presented in Eq. (4). The proposed mechanism is further supported by the applied kinetic equation that is developed considering the experimental data. Table 1 provides the temperature dependencies of the kinetic parameters.

$$r_{CH_4} = \frac{K_1\, k_2\, k_3\, p_{CH_4}\, p_{CO_2}}{K_1\, k_3\, p_{CH_4}\, p_{CO_2} + K_1\, k_2\, p_{CH_4} + k_3\, p_{CO_2}} \tag{4}$$

2.3 Kinetic rate model of Ru/La_2O_3 catalyst

Carrara et al. [22] utilized the Ru/La_2O_3 catalyst and proceeded to determine the rate constant for the DRM reaction at atmospheric pressure (510–590 °C) and experimented under various CO_2/CH_4 partial pressure ratios. Particularly, the temperature range that selected was also in line with the known operating range of the Ru catalyst. The applied mechanism of the reaction for Ru/La_2O_3, once introduced for Ni/La_2O_3 by Tsipouriari and Verykios [23] and subsequently adopted for Rh-based catalysts by Múnera et al. [20, 21], is based on a significant role of the support

Table 1 The temperature dependencies of the kinetic parameters for Eqs. (3)–(9)

Equation	Kinetic parameters	Units	Ref.
Eq. (3)	$K_1 = 1.4 \times 10^3 \times \exp(-3930/T)$	(bar^{-1})	[20]
	$k_2 = 2.44 \times \exp(-8549/T)$	(mol g_{cat}^{-1} s^{-1})	
	$k_3 = 1.2 \times \exp(-4990/T)$	(mol g_{cat}^{-1} s^{-1} bar^{-1})	
Eq. (4)	$K_1 = 1.94 \times 10^{-2} \times \exp(4550/T)$	(bar^{-1})	[21]
	$k_2 = 419.4 \times \exp(-11111/T)$	(mol g_{cat}^{-1} s^{-1})	
	$k_3 = 102.3 \times \exp(-231.6/T)$	(mol g_{cat}^{-1} s^{-1} bar^{-1})	
Eq. (5)	$K_1 = 1.46 \times 10^{-4} \times \exp(7242/T)$	(bar^{-1})	[22]
	$k_2 = 2.94 \times 10^3 \times \exp(-12949/T)$	(mol g_{cat}^{-1} s^{-1})	
	$k_3 = 4.05 \times 10^{10} \times \exp(15891/T)$	(mol g_{cat}^{-1} s^{-1} bar^{-1})	
Eq. (6)	$k_1 = 1.35 \times 10^{-4} \times \exp(-25900/RT)$	(mol^2 g_{cat}^{-2} s^{-2} bar^{-2})	[26]
	$k_2 = 9.25 \times 10^{-6} \times \exp(40600/RT)$	(mol g_{cat}^{-1} s^{-1} bar^{-1})	
	$k_3 = 2.46 \times 10^{-5} \times \exp(38300/RT)$	(mol g_{cat}^{-1} s^{-1} bar^{-1})	
Eq. (7)	$K_1 = 2.9755 \times 10^4 \times \exp(-7502.5/T)$	(bar^{-1})	[24]
	$k_2 = 12.27 \times \exp(-10219.2/T)$	(mol g_{cat}^{-1} s^{-1})	
	$k_3 = 3.4 \times \exp(-4990/T)$	(mol g_{cat}^{-1} s^{-1} bar^{-1})	
Eq. (8)	$K_1 = 7.82 \times 10^{-4}$ $\exp(8280/T)$	(bar^{-1})	[25]
	$k_2 = 4800 \times \exp(-16470/T)$	(mol g_{cat}^{-1} s^{-1})	
	$K_3 = 7.54 \times 10^{-5} \times \exp(9200/T)$	(bar^{-1})	
	$k_4 = 632 \times \exp(-12110/T)$	(mol g_{cat}^{-1} s^{-1})	
Eq. (9)	$k_1 = 350$ $\exp(-9746/T)$	(mol g_{cat}^{-1} s^{-1})	[34–36]
	$K_2 = 0.5771$ $\exp(1114/T)$	(bar^{-1})	
	$K_3 = 1.494$ $\exp(724.7/T)$	(bar^{-1})	
	$K_{RWGS} = 56.4971$ $\exp(-4340/T)$		

material (La_2O_3) in the reaction. The kinetic rate model is presented in Eq. (5) and the temperature dependencies of the kinetic parameters provided on Table 1.

$$r_{CH_4} = \frac{K_1 k_2 k_3 p_{CH_4} p_{CO_2}}{K_1 k_3 p_{CH_4} p_{CO_2} + K_1 k_2 p_{CH_4} + k_3 p_{CO_2}} \quad (5)$$

2.4 Kinetic rate model of Ni-Co/Al-Mg-O catalyst

Kinetic studies on the Ni-Co/Al-Mg-O bimetallic catalyst were conducted under 3.1 bar and 650–750 °C with varying CO_2/CH_4 ratio in another study by Zhang et al. [26]. The proposed mechanism includes CH_4 dissociation and surface carbon with activated CO_2 as rate-limiting steps. Eq. (4) presents the kinetic rate model, and Table 1 provides the temperature dependencies of the kinetic parameters. This model aligns experimental values with theoretical calculations.

$$r_{CH_4} = \frac{k_1 p_{CH_4} p_{CO_2}}{k_2 p_{CH_4} + k_3 p_{CO_2}} \quad (6)$$

2.5 Kinetic rate model of $LaNiO_3$ perovskite catalyst

The exploration of the kinetic studies in DRM reaction over $LaNiO_3$ was done by Moradi et al. [24] at atmospheric pressure (650–750 °C) with changing CO_2/CH_4 partial pressure ratios. The proposed mechanism resembling the Ni/La_2O_3 system [23] consists of four sequential steps: reversible adsorption and cracking of CH_4; CO_2 activation on La_2O_3 leading to oxycarbonate species formation; and final slow reaction between surface carbon and CO_2 at metal-oxide interface. The kinetic rate model is presented in Eq. (7). Table 1 provides the temperature dependencies of the kinetic parameters.

$$r_{CH_4} = \frac{K_1 k_2 k_3 p_{CH_4} p_{CO_2}}{K_1 k_3 p_{CH_4} p_{CO_2} + K_1 k_2 p_{CH_4} + k_3 p_{CO_2}} \quad (7)$$

2.6 Kinetic rate model of Ce-La-Ni-O_2 catalyst

Pino et al. [25] evaluated the thermodynamics and kinetics of the DRM process over $Ce_{0.7}La_{0.2}Ni_{0.1}O_{2-\delta}$ catalyst under atmospheric pressure (650–750 °C) with varying CO_2/CH_4 ratios. The proposed mechanism involves co-adsorption of CO_2 and CH_4 on nickel sites and La_2O_3 support, with the rate-limiting step is surface reactions. CO_2 activation on the support forms $La_2O_2CO_3$ compounds, which react with surface carbon to produce CO, regenerating active sites. The kinetic rate model is given in Eq. (8), and Table 1 shows the temperature dependencies of the kinetic parameters.

$$r_{CH_4} = \frac{K_1\, k_2\, K_3\, k_4\, p_{CH_4}\, p_{CO_2}}{K_3\, k_4\, p_{CO_2} + K_1\, K_3\, k_4\, p_{CH_4}\, p_{CO_2} + K_1\, k_2\, p_{CH_4} + K_1\, k_2\, K_3\, p_{CO_2}} \tag{8}$$

2.7 Kinetic rate models of RWGS reaction

Equations (3)–(8) present kinetic rate models for the six studied catalysts, excluding the RWGS reaction, as it typically parallels the DRM reaction and operates at equilibrium [8, 15–22, 24–26]. Therefore, the RWGS kinetic rate model and parameters were sourced from other studies [34–36], as shown in Eq. (9) and Table 1.

$$r_{CO_2} = \frac{k_1\, K_2\, K_3\, p_{CO_2}\, p_{H_2}}{\left(1 + K_2\, p_{CO_2} + K_3\, p_{H_2}\right)^2} \times \frac{K_{RWGS}\, p_{CO_2}\, p_{H_2} - p_{H_2O}\, p_{CO}}{K_{RWGS}\, p_{CO_2}\, p_{H_2}} \tag{9}$$

Equations (3)–(8) neglect the reverse reactions, and thus are suitable for short reactors. However, this simulation involves a longer reactor where reverse reactions are significant. Consequently, Eqs. (3)–(8) must incorporate reverse reactions by integrating Eqs. (10)–(11) into the kinetic rate model, providing sufficient accuracy for most modeling applications [32, 34–36]:

$$r_{CH_4} = \frac{K_{DRM}\, p_{CH_4}\, p_{CO_2} - \left(p_{CO}\, p_{H_2}\right)^2}{K_{DRM}\, p_{CH_4}\, p_{CO_2}}, \tag{10}$$

where:

$$K_{DRM} = 6.78 \times 10^{14} \exp\left(-\frac{31232}{T}\right). \tag{11}$$

3 Simulation methodology

The following chapter specifies the main underpinnings of the simulation model. This set of presumptions relates to the type of a chosen model, the component definitions of the selected systems, the considered unit operations, and the utilization of the streamlining techniques for the sake of efficiency of the calculations.

3.1 Assumptions for simulation

This study adopted the following simplifying assumptions for the simulation:

- Pure biogas feed: the CH_4 and CO_2 composition of the biogas stream that enters the reformer was supposed to be an entirely pure gas, free of any impurity species.
- Reliable property prediction: the software's built-in physical property model aimed to accurately replicate real-world behavior of chosen components under realistic operating conditions.
- Realistic catalyst representation: This means that the catalyst properties assumed in the simulation are considered to represent actual catalytic conditions in the DRM process.
- Fixed bed reactor configuration: since this type of catalytic process typically uses a fixed-bed reactor design, the reformer was scaled accordingly.
- Negligible carbon formation: considering that spent catalysts produce negligible or almost no carbon, the reaction that is described in Eq. (2) (RWGS reaction) is considered to be the only side reaction that is occurring at the reformer [26].

3.2 Process simulation approach

The DWSIM v8.6.7 simulation software [27] was applied in this work to simulate a process that involves 5000 kmol h^{-1} of biogas. In the simulated process, there were three material streams and two unit operation modules. Fig. 2 is a simplified flow diagram of the process which describes the next sections in more detail.

3.3 Component definition and method

The stream conditions tab in the software allows defining the stream's overall state, present phases, component parameters, and property calculation method. All components were defined as vapor-liquid equilibrium (VLE), with physical properties specified using the built-in database. The Peng-Robinson equation of state, known for its effectiveness in calculating vapor-liquid equilibrium under pressure, was employed in this study [37]. Eqs. (3)–(9) and the parameters in Table 1 was transformed into a form that is compatible with DWSIM. Table A1 (in the Appendix)

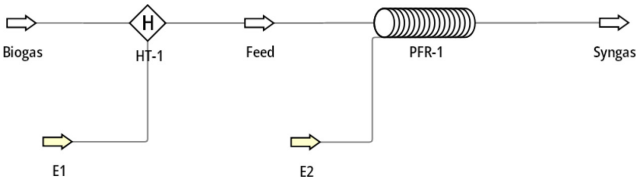

Fig. 2 Simple flowsheet of the dry-reforming of biogas process

presents the rate model that was adjusted and used for simulation in the DWSIM.

3.4 Unit operation and streamline

The process simulation (Fig. 2) includes three material streams (biogas input, feed stream, syngas product) and two unit operations (heater HT-1, reformer PFR-1). Initially, the biogas stream enters the heater (HT-1) for preheating to 750 °C, becoming the feed stream. This hottest feed stream then enters the reformer (PFR-1) where DRM conversion occurs, producing the syngas stream. Table 2 provides detailed operation conditions for all streams and units in the simulation.

4 Simulation results and discussion

The effect of pressure, CH_4/CO_2 ratio in feed (FR), and temperature on the conversion of CO_2 and CH_4 (denoted X_{CO_2} and X_{CH_4}, respectively) and the resulting ratio of the H_2/CO in the syngas product stream will be investigated in this section. A comparison of all catalysts will also be included in the analysis.

4.1 Effect of temperature

To investigate the impact of temperature on the X_{CH_4}, X_{CO_2}, and H_2/CO ratio in the syngas, simulations were conducted under the operating conditions outlined in Table 2. For a sensitivity analysis, a series of simulations were performed in DWSIM at five distinct conditions: 550, 600, 650, 700, and 750 °C. The findings of this simulation are presented in Fig. 3.

Fig. 3 indicates the output product and reaction temperature have a straight-line relationship. The process of converting CH_4 and CO_2 increases correspondingly with temperature [38]. It implies that the reactions described in Eqs. (1) and (2), which are generally accepted to show an endothermic nature at high temperatures [39–41], further support the idea that such reactions are thermodynamically more favorable at high temperatures. As shown in Fig. 3, X_{CO_2} dominates over X_{CH_4} consistently. The above point proves that the existence of RWGS (Eq. (2)) will increase X_{CO_2}. This characteristic arises because CO_2 plays dual roles, participating in both the DRM (Eq. (1)) and the RWGS (Eq. (2)) reaction, whereas CH_4 is only involved in the DRM reaction. The existence of the interaction between DRM (Eq. (1)), which forms H_2 and CO with a steady ratio of 1:1, and the RWGS reaction (Eq. (2)), which produces CO and consumes H_2, should cause the H_2/CO ratio to decrease with temperature. It's interesting to note that for all catalysts, the syngas's H_2/CO ratio rises with temperature while remaining below 1. Fig. 4 can explain the finding.

The trend shows that the H_2 formation line in the reaction rate of DRM consistently rises above the consumption line in the reaction rate of RWGS. In addition, both reactions also form CO, with the net formation rate slightly above H_2 formation rate; hence, the H_2/CO ratio is always below 1.

Fig. 5 shows that catalysts have very different activities. In the entire range of temperatures, Rh/La_2O_3-SiO_2 and Ru/La_2O_3 exhibit the highest conversions, so they are the best for this particular application. Ni-Co/Mg-Al-O demonstrates good activity at lower temperatures (550–650 °C), with the conversions being as good as Rh/La_2O_3. In the high-temperature range (700–750 °C), Ni-Co/Mg-Al-O continues the satisfactory conversion, Rh/La_2O_3 and $LaNiO_3$ follow that. However, Ce-La-Ni-O_2 maintains the lowest productivity values across the whole temperature range.

Table 2 Operational parameters used in the simulation

Parameters	Unit	Biogas	HT-1	Feed	PFR-1	Syngas
Temperature	°C	50	–	750	Isothermic	750
Pressure	bar	1	–	1	–	0.9
Molar flow	kmol h^{-1}	5000	–	5000	–	8733.49
Pressure drop	bar	–	0	–	0.1	–
Volume	m^3	–	–	–	15	–
Tube length	m	–	–	–	12.52	–
Catalyst diameter	mm	–	–	–	0.2	–
Catalyst void fraction	–	–	–	–	0.6	–
Catalyst loading	kg m^{-3}	–	–	–	1000	–
Tube diameter	mm	–	–	–	87.33	–
Number of tubes	–	–	–	–	200	–
Efficiency	%	–	100	–	–	–
Outlet temperature	°C	–	750	–	750	–

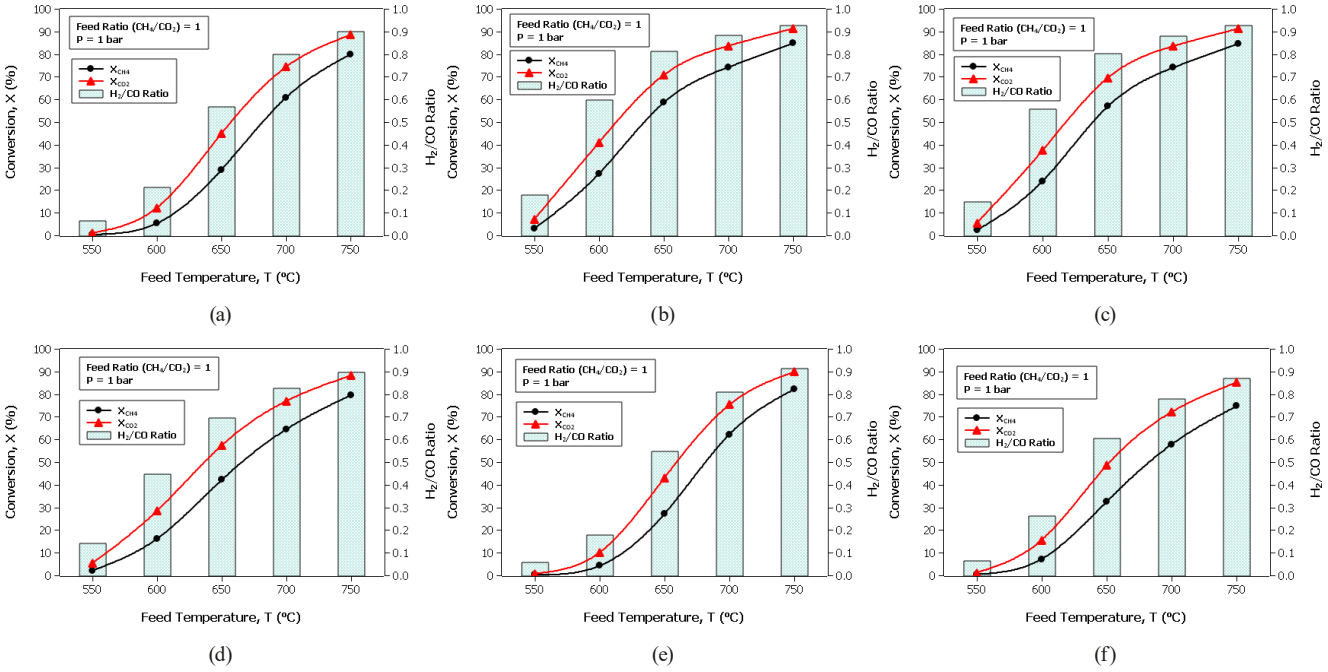

Fig. 3 Feed temperature effect on H_2/CO ratio, X_{CH_4}, and X_{CO_2}, at CH_4/CO_2 feed ratio = 1 and P = 1 bar for six catalysts; (a) Rh/La_2O_3 catalyst; (b) Rh/La_2O_3-SiO_2 catalyst; (c) Ru/La_2O_3 catalyst; (d) Ni-Co/Al-Mg-O catalyst; (e) $LaNiO_3$ catalyst; (f) Ce-La-Ni-O_2 catalyst

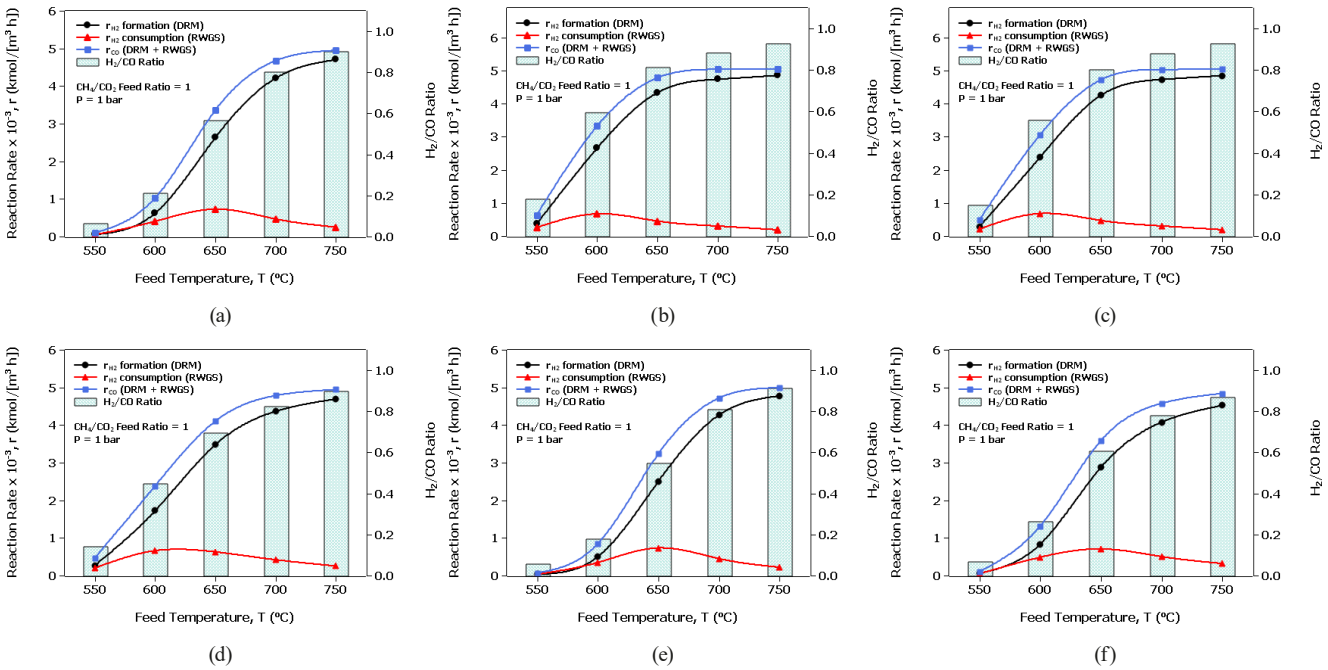

Fig. 4 The effect of feed temperature on r_{H_2} formation, r_{H_2} consumption, r_{CO}, and H_2/CO ratio at P = 1 bar and CH_4/CO_2 feed ratio = 1 for six catalysts; (a) Rh/La_2O_3 catalyst; (b) Rh/La_2O_3-SiO_2 catalyst; (c) Ru/La_2O_3 catalyst; (d) Ni-Co/Al-Mg-O catalyst; (e) $LaNiO_3$ catalyst; (f) Ce-La-Ni-O_2 catalyst

4.2 Effect of pressure

To look into the impact of pressure, the next set of simulations was run at 5 different pressure values in DWSIM: 1, 2, 3, 4, and 5 bar. As in the temperature analysis, this modeling aims to provide a sensitivity analysis with the conditions represented in Table 2. The pressure-related findings are demonstrated in Fig. 6.

Fig. 6 shows the negative influence of pressure on both X_{CH_4} and X_{CO_2} and also the decreasing H_2/CO ratio with increasing pressure at a constant temperature of 750 °C. It follows that X_{CH_4} and X_{CO_2} are limited at higher pressures. The evidence from numerous studies on the negative influence of pressure on both X_{CH_4} and X_{CO_2} and also the decreasing H_2/CO ratio with increasing pressure

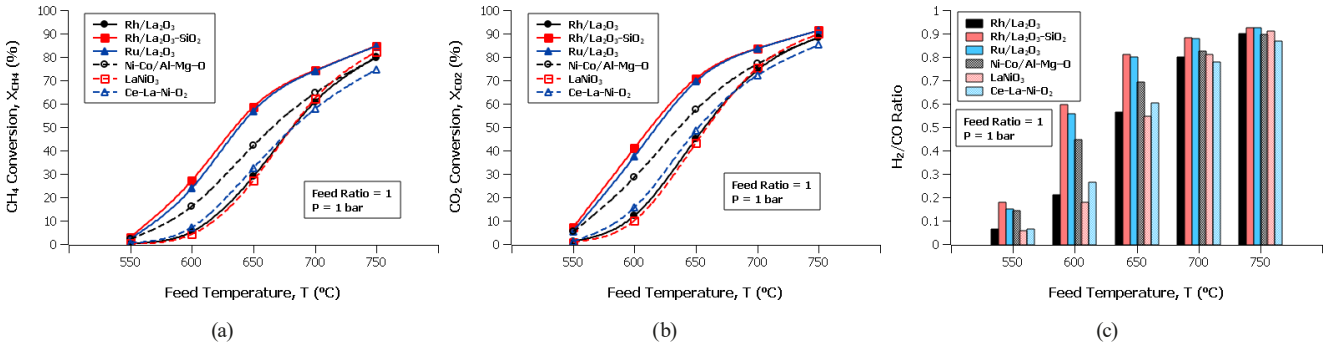

Fig. 5 Catalysts comparison for the effect of feed temperature at P = 1 bar, CH_4/CO_2 feed ratio = 1: (a) X_{CH_4}, (b) X_{CO_2}, and (c) H_2/CO ratio

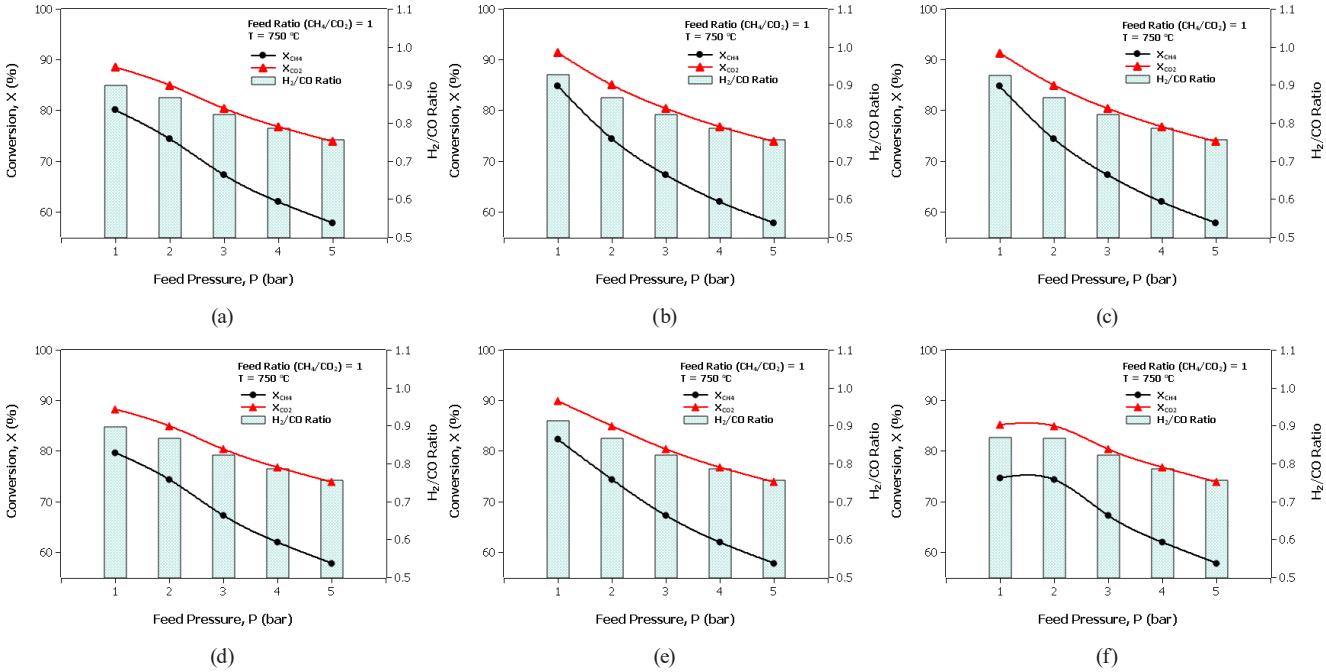

Fig. 6 Feed pressure effect on H_2/CO ratio, X_{CH_4}, and X_{CO_2}, at T = 750 °C and CH_4/CO_2 feed ratio = 1 for six catalysts; (a) Rh/La_2O_3 catalyst; (b) Rh/La_2O_3-SiO_2 catalyst; (c) Ru/La_2O_3 catalyst; (d) Ni-Co/Al-Mg-O catalyst; (e) $LaNiO_3$ catalyst; (f) Ce-La-Ni-O_2 catalyst

is a fact [42–46]. Despite low conversion, a high-pressure reactor in one study showed potential for better energy efficiency [43]. The process can be more efficient by having extra CO_2 and H_2 [44, 45]. In addition, an excess CO_2/CH_4 ratio over the stoichiometric value is optional to achieve a high X_{CH_4} at high pressures [47].

Fig. 7 shows the comparison of all six catalysts at T = 750 °C and CH_4/CO_2 feed ratio = 1 with varying pressure. The observation that at 1 bar, the Ru/La_2O_3 and Rh/La_2O_3-SiO_2 catalysts exhibit superior performance in terms of X_{CH_4} (Fig. 7(a)), X_{CO_2} (Fig. 7(b)), and H_2/CO ratio (Fig. 7(c)) compared to the other catalysts, but at pressures from 2 to 5 bar, all catalysts converge to the same values, is quite intriguing. At 1 bar pressure, Ru/La_2O_3 and Rh/La_2O_3-SiO_2 catalysts demonstrate superior performance in H_2/CO ratio, X_{CH_4}, and X_{CO_2} compared to other catalysts, possibly due to enhanced kinetics, such as their better active site availability, improved metal-support interactions, and more efficient reactant activation [48, 49]. To confirm this, an examination of the apparent activation energy (E_{ap}) of each catalyst is warranted. The E_{ap} can be estimated from Arrhenius plots (T^{-1} vs. ln (k), not illustrated here). The E_{ap} of each catalyst is listed in Table 3.

A lower E_{ap} indicates a higher catalytic activity of the catalyst. As can be seen in Table 3, the Ru/La_2O_3 and Rh/La_2O_3-SiO_2 catalysts have the smallest E_{ap} value compared to the other catalysts. This confirms the superior performance of the Ru/La_2O_3 and Rh/La_2O_3-SiO_2 catalysts. Nonetheless, between the pressures of 2 and 5 bar, all catalysts manifest the same performance, pointing to the emerging thermodynamic control where equilibrium has a domineering effect [50], as shown by equilibrium line in Fig. 7. This thermodynamic limitations take over the kinetic advantages at higher pressures, which may give

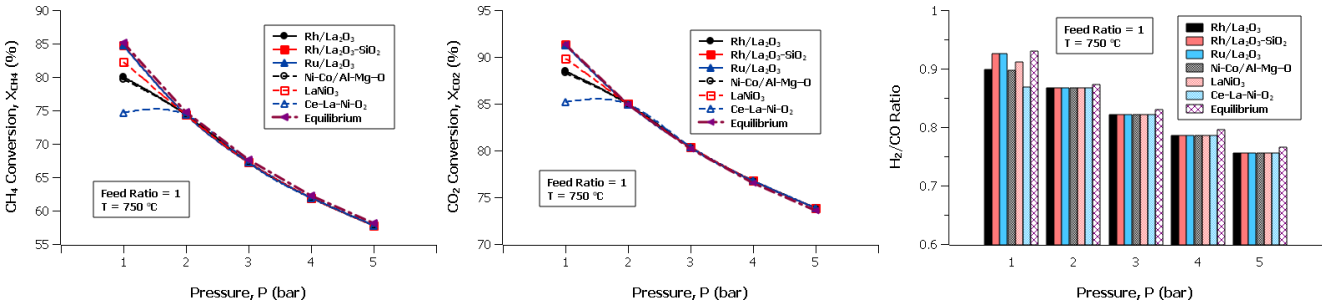

(a) (b) (c)

Fig. 7 Catalysts comparison for the effect of feed pressure at T = 750 °C, CH_4/CO_2 feed ratio = 1: (a) X_{CH_4}, (b) X_{CO_2}, and (c) H_2/CO ratio

Table 3 Comparison of E_{ap} (kJ mol^{-1}) for all catalysts

Catalyst	E_{ap} (CH_4)
Rh/La_2O_3	90.61
Rh/La_2O_3-SiO_2	67.76
Ru/La_2O_3	60.42
Ni-Co/Al-Mg–O	68.90
$LaNiO_3$	92.23
Ce-La-Ni-O_2	73.06

rise to deactivation mechanisms, changes in mass transfer, or changes in the adsorption-desorption behavior of reactants and products that affect reaction rates and selectivity [51–53]. The interplay between kinetic and thermodynamic factors in the dry reforming of biogas reactions concerning different pressures manifests the intricacy of catalyst function at various scales of pressure levels.

4.3 Effect of feed ratio (CH_4/CO_2)

The sensitivity analysis to the feed ratio (CH_4/CO_2) with conditions such as in Table 2 is done by simulating the five feed ratios: 1, 1.25, 1.5, 1.75, and 2. The results of the simulation can be seen in Fig. 7.

Fig. 8 illustrates the consequences of different CH_4/CO_2 feed ratios at 750 °C and 1 bar pressure on the biogas reforming of methane reaction. As Fig. 8 illustrates, a higher CH_4/CO_2 feed ratio result in a higher X_{CO_2} but a lower X_{CH_4}. This is because CH_4 is in excess, which makes the reaction shift towards the product side according to Le Chatelier's principle [46, 49, 54–56]. Nevertheless, an intriguing pattern showed up: even though X_{CH_4} was declining, the ratio of H_2/CO increased along the CH_4/CO_2 feed ratio. The explanation for this is depicted in Fig. 9.

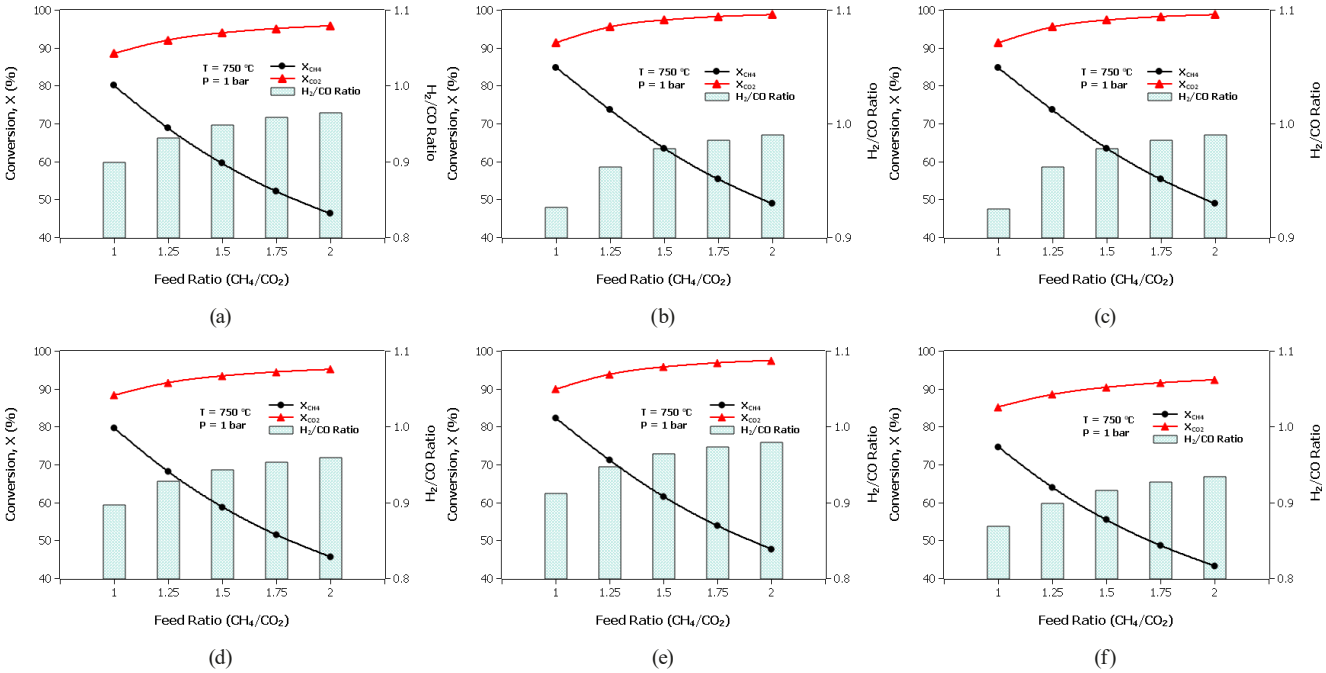

(a) (b) (c)

(d) (e) (f)

Fig. 8 CH_4/CO_2 feed ratio effect on H_2/CO ratio, X_{CO_2}, and X_{CH_4} at T = 750 °C and P = 1 bar for six catalysts; (a) Rh/La_2O_3 catalyst; (b) Rh/La_2O_3-SiO_2 catalyst; (c) Ru/La_2O_3 catalyst; (d) Ni-Co/Al-Mg-O catalyst; (e) $LaNiO_3$ catalyst; (f) Ce-La-Ni-O_2 catalyst

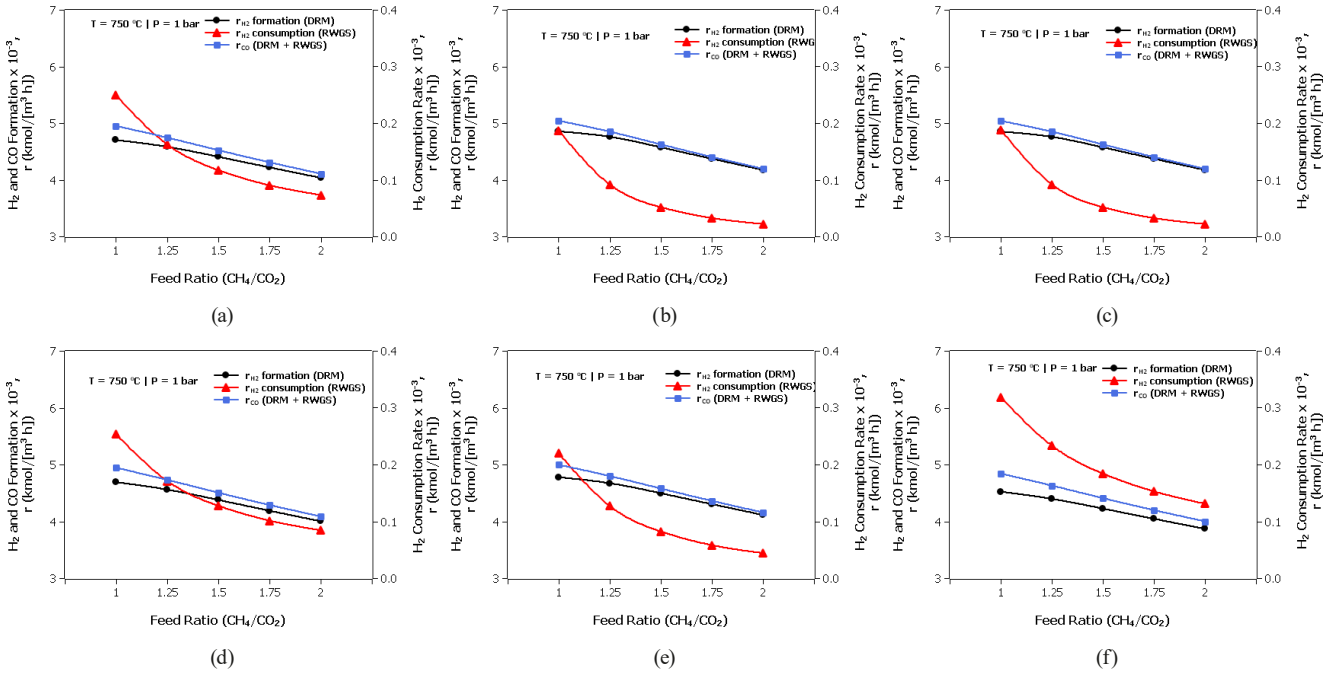

Fig. 9 CH_4/CO_2 feed ratio effect on r_{H_2} formation, r_{H_2} consumption, r_{CO}, and H_2/CO ratio at $T = 750$ °C and $P = 1$ bar for six catalysts; (a) Rh/La_2O_3 catalyst; (b) Rh/La_2O_3-SiO_2 catalyst; (c) Ru/La_2O_3 catalyst; (d) Ni-Co/Al-Mg-O catalyst; (e) $LaNiO_3$ catalyst; (f) Ce-La-Ni-O_2 catalyst

As illustrated in Fig. 9, for all catalysts, the rate of H_2 formation (the black line + circle) from the DRM reaction decreases with an increasing CH_4/CO_2 feed ratio, following expectations based on lower X_{CH_4}. In addition, the rate of CO formation (the blue line + square) from both the DRM and RWGS reactions also decreases with higher feed ratios. Nonetheless, the rate of H_2 consumption via the RWGS reaction (the red line + triangle) decreases significantly when the CH_4/CO_2 ratio increases. The observed decline in the RWGS reaction rate can be explained by the increase in the CH_4 concentration, which reduces the reaction rate. These findings indicated that the DRM reaction competed with the RWGS reaction for the availability of CO_2.

It is reasonable to conclude that the RWGS reaction will be suppressed when additional CH_4 is present since the equilibrium constant K of the RWGS is significantly lower than that of the DRM reaction [26].

This reduction in H_2 consumption, coupled with the continued production of H_2 (with a smaller decrease compared to H_2 consumption) from the DRM reaction (the black line + circle), results in a net increase in the ratio of H_2/CO, as illustrated in Fig. 8 (the blue bar). Although the ratio of H_2/CO increases at high CH_4/CO_2 feed ratios, the % yield of H_2 is smaller, as shown in Table 4. The findings of the study by Albano et al. [49] are consistent with this finding.

The comparison of all six catalysts at $T = 750$ °C and $P = 1$ bar across various CH_4/CO_2 feed ratio demonstrated in Fig. 10. Although X_{CH_4} decreased with increasing CH_4/CO_2 feed ratio, Rh/La_2O_3-SiO_2 and Ru/La_2O_3 exhibit the highest performance in terms of X_{CH_4} (Fig. 10(a)), X_{CO_2} (Fig. 10(b)), and H_2/CO ratio (Fig. 10(c)), maintaining nearly 100% X_{CO_2} conversion and H_2/CO ratios close to 1.0. $LaNiO_3$ performs moderately well, better than Ni-Co/Al-Mg-O and Rh/La_2O_3, but not as effectively

Table 4 CH_4/CO_2 feed ratio vs. % yield of H_2 for all catalysts at $T = 750$ °C and $P = 1$ bar

CH_4/CO_2 feed ratio	% yield of H_2					
	Rh/La_2O_3	Rh/La_2O_3-SiO_2	Ru/La_2O_3	Ni-Co/Al-Mg–O	$LaNiO_3$	Ce-La-Ni-O_2
1	75.76	81.53	81.4	75.34	78.5	69.41
1.25	66.33	72.17	72.14	65.62	69.24	60.61
1.5	57.89	62.73	62.73	57.11	60.46	53
1.75	50.97	54.89	54.89	50.22	53.13	46.8
2	45.38	48.59	48.59	44.67	47.2	41.78

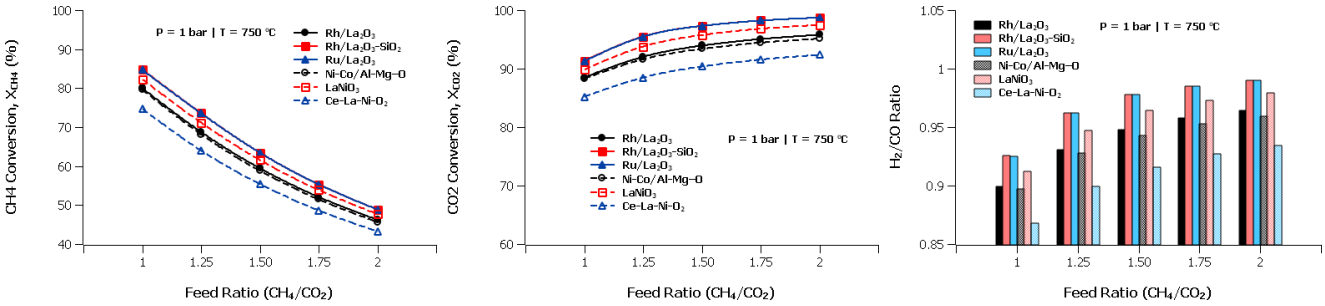

(a) (b) (c)

Fig. 10 Catalysts comparison for the effect of CH_4/CO_2 feed ratio at T = 750 °C and P = 1 bar: (a) X_{CH_4}, (b) X_{CO_2}, and (c) H_2/CO ratio

as Rh/La_2O_3-SiO_2 and Ru/La_2O_3. Ni-Co/Al-Mg-O and Rh/La_2O_3 show similar, slightly lower performance, while Ce-La-Ni-O_2 has the lowest conversions and H_2/CO ratios among the tested catalysts.

5 Conclusion

Dry reforming of biogas offers a promising method for generating syngas with a flexible H_2/CO ratio suitable for various chemical production processes. This study investigated the effects of CH_4/CO_2 feed ratio, pressure, and temperature on the X_{CH_4}, X_{CO_2}, and syngas product's H_2/CO ratio for six different catalysts using simulations. The simulations revealed that higher temperatures up to 750 °C are more suitable for higher X_{CH_4}, X_{CO_2}, and H_2/CO ratio for all catalysts because of the endothermic nature of the reactions. Higher pressure had a negative effect, reducing both the conversion and the H_2/CO ratio. Rather intriguingly, all six catalysts showed a similar level of performance in the pressure range of 2–5 bar, indicating that thermodynamic constraints more significant compared to the kinetic factors at elevated pressures. Under lower pressures, the Ru/La_2O_3 and Rh/La_2O_3-SiO_2 catalysts had higher catalytic activity than the other catalysts, due to their favorable kinetics. This is corroborated by the minimal E_{ap} value relative to other catalysts (Table 3). But, at higher pressures, thermodynamics played a significant role, and the catalysts' catalytic activities became equivalent (Fig. 7). A higher CH_4/CO_2 feed ratio decreased X_{CH_4}, increasing X_{CO_2} and the ratio of H_2/CO. However, at a higher CH_4/CO_2 molar ratio, the H_2 amount is decreased. The reduction in conversion of CH_4 and H_2 amounts due to CH_4 is in excess, which makes the reaction shift towards the product side according to Le Chatelier's principle.

Besides the catalytic performance, future research should also use value engineering techniques to choose the best catalyst by considering the economic conditions for the process of dry reforming. The total costs of catalyst production, usage, energy needs, and the capital and operating expenses for various catalyst-process combinations that give the desired syngas composition should be evaluated through deep techno-economic assessments. Renewable hydrogen injection to improve the H_2/CO ratio in syngas will be a future potential enhancement for more versatile syngas utilization. The whole research can demonstrate the most economical H_2/CO catalyst that at the same time meets the syngas productivity and the H_2/CO ratio requirements.

Nomenclature

K_1, K_2, K_3, K_{DRM}, K_{RWGS} = equilibrium constant
k_1, k_2, k_3, k_4 = reaction rate constant
r_{CH_4}, r_{CO_2}, r_{H_2}, r_{CO} = reaction rate
T = temperature
R = ideal gas constant
P = partial pressure

References

[1] Ereña, J. "Catalysts for Syngas Production", Catalysts, 10(6), 657, 2020. https://doi.org/10.3390/catal10060657

[2] He, M., Xiao, B., Liu, S., Hu, Z., Guo, X., Luo, S., Yang, F. "Syngas production from pyrolysis of municipal solid waste (MSW) with dolomite as downstream catalysts", Journal of Analytical and Applied Pyrolysis, 87(2), pp. 181–187, 2010. https://doi.org/10.1016/j.jaap.2009.11.005

[3] Rezaei, M., Alavi, S. M., Sahebdelfar, S., Yan, Z.-F. "Syngas Production by Methane Reforming with Carbon Dioxide on Noble Metal Catalysts", Journal of Natural Gas Chemistry, 15(4), pp. 327–334, 2006. https://doi.org/10.1016/S1003-9953(07)60014-0

[4] Gao, J., Guo, J., Liang, D., Hou, Z., Fei, J., Zheng, X. "Production of syngas via autothermal reforming of methane in a fluidized-bed reactor over the combined CeO_2–ZrO_2/SiO_2 supported Ni catalysts", International Journal of Hydrogen Energy, 33(20), pp. 5493–5500, 2008. https://doi.org/10.1016/j.ijhydene.2008.07.040

[5] EPA "EPA Issues Final Rule for Renewable Fuel Standard (RFS) Pathways II and Modifications to the RFS Program, Ultra Low Sulfur Diesel Requirements, and E15 Misfueling Mitigation Requirements", United States Environmental Protection Agency, Washington, DC, USA, Rep. EPA-420-F-14-045, 2014.

[6] Zhao, X., Joseph, B., Kuhn, J., Ozcan, S. "Biogas Reforming to Syngas: A Review", iScience, 23(5), 101082, 2020. https://doi.org/10.1016/j.isci.2020.101082

[7] Xu, J., Zhou, W., Li, Z., Wang, J., Ma, J. "Biogas reforming for hydrogen production over nickel and cobalt bimetallic catalysts", International Journal of Hydrogen Energy, 34(16), pp. 6646–6654, 2009. https://doi.org/10.1016/j.ijhydene.2009.06.038

[8] Singh, R., Dhir, A., Mohapatra, S. K., Mahla, S. K. "Dry reforming of methane using various catalysts in the process: review", Biomass Conversion and Biorefinery, 10(2), pp. 567–587, 2020. https://doi.org/10.1007/s13399-019-00417-1

[9] Ritzen, L., Sprecher, B., Bakker, C., Balkenende, R. "Bio-based plastics in a circular economy: A review of recovery pathways and implications for product design", Resources, Conservation and Recycling, 199, 107268, 2023. https://doi.org/10.1016/j.resconrec.2023.107268

[10] Awe, O. W., Zhao, Y., Nzihou, A., Minh, D. P., Lyczko, N. "A Review of Biogas Utilisation, Purification and Upgrading Technologies", Waste and Biomass Valorization, 8(2), pp. 267–283, 2017. https://doi.org/10.1007/s12649-016-9826-4

[11] Rathod, V., Bhale, P. V. "Experimental Investigation on Biogas Reforming for Syngas Production over an Alumina based Nickel Catalyst", Energy Procedia, 54, pp. 236–245, 2014. https://doi.org/10.1016/J.EGYPRO.2014.07.267

[12] Charisiou, N. D., Douvartzides, S. L., Siakavelas, G. I., Tzounis, L., Sebastian, V., Stolojan, V., Hinder, S. J., Baker, M. A., Polychronopoulou, K., Goula, M. A. "The Relationship between Reaction Temperature and Carbon Deposition on Nickel Catalysts Based on Al_2O_3, ZrO_2 or SiO_2 Supports during the Biogas Dry Reforming Reaction", Catalysts, 9(8), 676, 2019. https://doi.org/10.3390/catal9080676

[13] Zhang, Q., Wang, J., Ning, P., Zhang, T., Wang, M., Long, K., Huang, J. "Dry reforming of methane over Ni/SBA-15 catalysts prepared by homogeneous precipitation method", Korean Journal of Chemical Engineering, 34(11), pp. 2823–2831, 2017. https://doi.org/10.1007/s11814-017-0182-2

[14] Kim, J., Kim, T., Yoo, J. W., Lee, K. B., Hong, S.-I. "Carbon dioxide reforming of methane to synthesis gas over $LaNi_{1-x}Cr_xO_3$ perovskite catalysts", Korean Journal of Chemical Engineering, 29(10), pp. 1329–1335, 2012. https://doi.org/10.1007/s11814-012-0057-5

[15] Bradford, M. C. J., Vannice, M. A. "CO_2 Reforming of CH_4", Catalysis Reviews, 41(1), pp. 1–42, 1999. https://doi.org/10.1081/CR-100101948

[16] Bradford, M. C. J., Vannice, M. A. "CO_2 Reforming of CH_4 over Supported Ru Catalysts", Journal of Catalysis, 183(1), pp. 69–75, 1999. https://doi.org/10.1006/jcat.1999.2385

[17] Bradford, M. C. J., Vannice, M. A. "CO_2 Reforming of CH_4 over Supported Pt Catalysts", Journal of Catalysis, 173(1), pp. 157–171, 1998. https://doi.org/10.1006/jcat.1997.1910

[18] Wei, J., Iglesia, E. "Isotopic and kinetic assessment of the mechanism of reactions of CH_4 with CO_2 or H_2O to form synthesis gas and carbon on nickel catalysts", Journal of Catalysis, 224(2), pp. 370–383, 2004. https://doi.org/10.1016/j.jcat.2004.02.032

[19] Barroso Quiroga, M. M., Castro Luna, A. E. "Kinetic Analysis of Rate Data for Dry Reforming of Methane", Industrial & Engineering Chemistry Research, 46(16), pp. 5265–5270, 2007. https://doi.org/10.1021/ie061645w

[20] Múnera, J. F., Irusta, S., Cornaglia, L. M., Lombardo, E. A., Vargas Cesar, D., Schmal, M. "Kinetics and reaction pathway of the CO_2 reforming of methane on Rh supported on lanthanum-based solid", Journal of Catalysis, 245(1), pp. 25–34, 2007. https://doi.org/10.1016/j.jcat.2006.09.008

[21] Múnera, J. F., Cornaglia, L. M., Cesar, D. V., Schmal, M., Lombardo, E. A. "Kinetic Studies of the Dry Reforming of Methane over the Rh/La_2O_3-SiO_2 Catalyst", Industrial & Engineering Chemistry Research, 46(23), pp. 7543–7549, 2007. https://doi.org/10.1021/ie061621p

[22] Carrara, C., Múnera, J., Lombardo, E. A., Cornaglia, L. M. "Kinetic and Stability Studies of Ru/La_2O_3 Used in the Dry Reforming of Methane", Topics in Catalysis, 51(1), pp. 98–106, 2008. https://doi.org/10.1007/s11244-008-9131-y

[23] Tsipouriari, V. A., Verykios, X. E. "Kinetic study of the catalytic reforming of methane with carbon dioxide to synthesis gas over Ni/La_2O_3 catalyst", Catalysis Today, 64(1–2), pp. 83–90, 2001. https://doi.org/10.1016/S0920-5861(00)00511-3

[24] Moradi, G. R., Rahmanzadeh, M., Sharifnia, S. "Kinetic investigation of CO_2 reforming of CH_4 over La–Ni based perovskite", Chemical Engineering Journal, 162(2), pp. 787–791, 2010. https://doi.org/10.1016/j.cej.2010.06.006

[25] Pino, L., Italiano, C., Laganà, M., Vita, A., Recupero, V. "Kinetic study of the methane dry (CO_2) reforming reaction over the $Ce_{0.70}La_{0.20}Ni_{0.10}O_{2-\delta}$ catalyst", Catalysis Science & Technology, 10(8), pp. 2652–2662, 2020. https://doi.org/10.1039/C9CY02192B

[26] Zhang, J., Wang, H., Dalai, A. K. "Kinetic Studies of Carbon Dioxide Reforming of Methane over Ni−Co/Al−Mg−O Bimetallic Catalyst", Industrial & Engineering Chemistry Research, 48(2), pp. 677–684, 2008. https://doi.org/10.1021/ie801078p

[27] Medeiros, D. "DWSIM: The Open Source Chemical Process Simulator, (8.6.7)", [computer program] Available at: https://dwsim.org/index.php/download/ [Accessed: 22 April 2024]

[28] Sigue, S., Abderafi, S., Vaudreuil, S., Bounahmidi, T. "Simulators Selection for Design and Simulation of a CSP-Driven Forward Osmosis Process", In: 2019 7th International Renewable and Sustainable Energy Conference (IRSEC), Agadir, Morocco, 2019, pp. 1–6. ISBN 978-1-7281-5152-6
https://doi.org/10.1109/IRSEC48032.2019.9078216

[29] Hassan, T. N., Manji, S. T. "Simulating Combined Cycle and Gas Turbine Power Plant under Design Condition using Open-Source Software DWSIM", ARO-The Scientific Journal of Koya University, 11(1), pp. 60–71, 2023.
https://doi.org/10.14500/aro.11098

[30] Tangsriwong, K., Lapchit, P., Kittijungjit, T., Klamrassamee, T., Sukjai, Y., Laoonual, Y. "Modeling of chemical processes using commercial and open-source software: A comparison between Aspen Plus and DWSIM", IOP Conference Series: Earth and Environmental Science, 463, 012057, 2020.
https://doi.org/10.1088/1755-1315/463/1/012057

[31] Andreasen, A. "Evaluation of an Open-source Chemical Process Simulator Using a Plant-wide Oil and Gas Separation Plant Flowsheet Model as Basis", Periodica Polytechnica Chemical Engineering, 66(3), pp. 503–511, 2022.
https://doi.org/10.3311/PPch.19678

[32] Zhao, Y. R., Latham, D. A., Peppley, B. A., McAuley, K. B., Wang, H., LeHoux, R. "Simulation of dry reforming of methane in a conventional downfired reformer", AIChE Journal, 63(6), pp. 2060–2071, 2017.
https://doi.org/10.1002/aic.15582

[33] Park, N., Park, M.-J., Baek, S.-C., Ha, K.-S., Lee, Y.-J., Kwak, G., Park, H.-G., Jun, K.-W. "Modeling and optimization of the mixed reforming of methane: Maximizing CO_2 utilization for non-equilibrated reaction", Fuel, 115, pp. 357–365, 2014.
https://doi.org/10.1016/j.fuel.2013.07.035

[34] Richardson, J. T., Paripatyadar, S. A. "Carbon dioxide reforming of methane with supported rhodium", Applied Catalysis, 61(1), pp. 293–309, 1990.
https://doi.org/10.1016/S0166-9834(00)82152-1

[35] Benguerba, Y., Dehimi, L., Virginie, M., Dumas, C., Ernst, B. "Modelling of methane dry reforming over Ni/Al_2O_3 catalyst in a fixed-bed catalytic reactor", Reaction Kinetics, Mechanisms and Catalysis, 114(1), pp. 109–119, 2015.
https://doi.org/10.1007/s11144-014-0772-5

[36] Benguerba, Y., Virginie, M., Dumas, C., Ernst, B. "Methane Dry Reforming over Ni-Co/Al_2O_3: Kinetic Modelling in a Catalytic Fixed-bed Reactor", International Journal of Chemical Reactor Engineering, 15(6), 20160170, 2017.
https://doi.org/10.1515/ijcre-2016-0170

[37] Dikwa, J., Ze Bilo'o, P., Allawadi, A. "Simulation of Dry Reforming of Methane Catalyzed by Iron Hexagonal Mesoporous Silicates (Fe-HMS) Using Aspen HYSYS", European Journal of Applied Sciences, 10(5), pp. 559–574, 2022.
https://doi.org/10.14738/aivp.105.13226

[38] Matus, E. V., Sukhova, O. B., Ismagilov, I. Z., Kerzhentsev, M. A., Li, L., Ismagilov, Z. R. "Bi-reforming of methane: thermodynamic equilibrium analysis and selection of preferable reaction conditions", Journal of Physics: Conference Series, 1749, 012023, 2021.
https://doi.org/10.1088/1742-6596/1749/1/012023

[39] Lavoie, J.-M. "Review on dry reforming of methane, a potentially more environmentally-friendly approach to the increasing natural gas exploitation", Frontiers in Chemistry, 2, 81, 2014.
https://doi.org/10.3389/fchem.2014.00081

[40] Serrano-Lotina, A., Daza, L. "Influence of the operating parameters over dry reforming of methane to syngas", International Journal of Hydrogen Energy, 39(8), pp. 4089–4094, 2014.
https://doi.org/10.1016/j.ijhydene.2013.05.135

[41] Simonov, M., Bespalko, Y., Smal, E., Valeev, K., Fedorova, V., Krieger, T., Sadykov, V. "Nickel-Containing Ceria-Zirconia Doped with Ti and Nb. Effect of Support Composition and Preparation Method on Catalytic Activity in Methane Dry Reforming", Nanomaterials, 10(7), 1281, 2020.
https://doi.org/10.3390/nano10071281

[42] Kahle, L. C. S., Roussière, T., Maier, L., Herrera Delgado, K., Wasserschaff, G., Schunk, S. A., Deutschmann, O. "Methane Dry Reforming at High Temperature and Elevated Pressure: Impact of Gas-Phase Reactions", Industrial & Engineering Chemistry Research, 52(34), pp. 11920–11930, 2013.
https://doi.org/10.1021/ie401048w

[43] Iwarere, S. A., Rohani, V.-J., Ramjugernath, D., Fulcheri, L. "Dry reforming of methane in a tip–tip arc discharge reactor at very high pressure", International Journal of Hydrogen Energy, 40(8), pp. 3388–3401, 2015.
https://doi.org/10.1016/j.ijhydene.2015.01.005

[44] Chein, R. Y., Chen, Y. C., Yu, C. T., Chung, J. N. "Thermodynamic analysis of dry reforming of CH_4 with CO_2 at high pressures", Journal of Natural Gas Science and Engineering, 26, pp. 617–629, 2015.
https://doi.org/10.1016/j.jngse.2015.07.001

[45] Chein, R. Y., Hsu, W. H., Yu, C. T. "Parametric study of catalytic dry reforming of methane for syngas production at elevated pressures", International Journal of Hydrogen Energy, 42(21), pp. 14485–14500, 2017.
https://doi.org/10.1016/j.ijhydene.2017.04.110

[46] Aimiuwu, G., Osagie, E., Omoregbe, O. "Process simulation for the production of methanol via CO_2 reforming of methane route", Chemical Product and Process Modeling, 17(1), pp. 69–79, 2022.
https://doi.org/10.1515/cppm-2020-0049

[47] Luyben, W. L. "Design and Control of the Dry Methane Reforming Process", Industrial & Engineering Chemistry Research, 53(37), pp. 14423–14439, 2014.
https://doi.org/10.1021/ie5023942

[48] Shopska, M., Kolev, H., Aleksieva, K., Shtereva, I., Tenchev, K., Todorova, S., Fabian, M., Kadinov, G. "Study of sites and species during CO hydrogenation over silica-supported Co–Pd catalysts. Relation to performance in the process", Reaction Kinetics, Mechanisms and Catalysis, 134(1), pp. 303–330, 2021.
https://doi.org/10.1007/s11144-021-02067-9

[49] Albano, M., Madeira, L. M., Miguel, C. V. "Use of Pd-Ag Membrane Reactors for Low-Temperature Dry Reforming of Biogas—A Simulation Study", Membranes, 13(7), 630, 2023.
https://doi.org/10.3390/membranes13070630

[50] Landa, L., Remiro, A., Valecillos, J., Bilbao, J., Gayubo, A. G. "Thermodynamic study of the CO_2 valorization in the combined steam-dry reforming of bio-oil into syngas", Journal of CO2 Utilization, 72, 102503, 2023. https://doi.org/10.1016/j.jcou.2023.102503

[51] Ahmad, W., Al-Matar, A., Shawabkeh, R., Aslam, Z., Malik, I. A., Irshad, H. M. "Cu-K/Al_2O_3 based catalysts for conversion of carbon dioxide to methane and carbon monoxide", Chemical Engineering Communications, 207(7), pp. 946–960, 2020. https://doi.org/10.1080/00986445.2019.1631815

[52] Grabchenko, M., Pantaleo, G., Puleo, F., Vodyankina, O., Liotta, L. F. "Ni/La_2O_3 catalysts for dry reforming of methane: Effect of La_2O_3 synthesis conditions on the structural properties and catalytic performances", International Journal of Hydrogen Energy, 46(11), pp. 7939–7953, 2021. https://doi.org/10.1016/j.ijhydene.2020.12.026

[53] Zhou, R., Mahinpey, N. "A review on catalyst development for conventional thermal dry reforming of methane at low temperature", The Canadian Journal of Chemical Engineering, 101(6), pp. 3180–3212, 2023. https://doi.org/10.1002/cjce.24876

[54] Zhu, X., Li, K., Liu, J.-L., Li, X.-S., Zhu, A.-M. "Effect of CO_2/CH_4 ratio on biogas reforming with added O_2 through an unique spark-shade plasma", International Journal of Hydrogen Energy, 39(25), pp. 13902–13908, 2014. https://doi.org/10.1016/j.ijhydene.2014.01.040

[55] Tang, Y., Li, Y., Bao, W., Yan, W., Zhang, J., Huang, Y., Li, H., Wang, Z., Liu, M., Yu, F. "Enhanced dry reforming of CO_2 and CH_4 on photothermal catalyst Ru/$SrTiO_3$", Applied Catalysis B: Environmental, 338, 123054, 2023. https://doi.org/10.1016/j.apcatb.2023.123054

[56] Benguerba, Y., Dehimi, L., Virginie, M., Dumas, C., Ernst, B. "Numerical investigation of the optimal operative conditions for the dry reforming reaction in a fixed-bed reactor: role of the carbon deposition and gasification reactions", Reaction Kinetics, Mechanisms and Catalysis, 115(2), pp. 483–497, 2015. https://doi.org/10.1007/s11144-015-0849-9

Appendix

Table A1 DRM and RWGS kinetic rate model input in DWSIM

Kinetic rate model	Equation
DRM kinetic rate model	
$r_{CH_4} = \frac{K_1 k_2 k_3 p_{CH_4} p_{CO_2}}{K_1 k_3 p_{CH_4} p_{CO_2} + K_1 k_2 p_{CH_4} + k_3 p_{CO_2}} \times \frac{K_{DRM} p_{CH_4} p_{CO_2} - (p_{CO} p_{H_2})^2}{K_{DRM} p_{CH_4} p_{CO_2}}$ **Numerator:** 1.4e+3 × exp(−3930/T) × 2.44 × exp(−8549/T) × 1.2 × exp(−4990/T) × R_1 × R_2 × (6.78e+14 × exp(−31232/T) × R_1 × R_2−(P_1 × P_2)^2) **Denominator:** 1.4e+3 × exp(−3930/T) × 1.2 × exp(−4990/T) × R_1 × R_2 + 1.4e+3 × exp(−3930/T) × 2.44 × exp(−8549/T) × R_1 + 1.2 × exp(−4990/T) × R_2 × (6.78e + 14 × exp(−31232/T) × R_1 × R_2)	Eq. (3) × Eq. (10)
$r_{CH_4} = \frac{K_1 k_2 k_3 p_{CH_4} p_{CO_2}}{K_1 k_3 p_{CH_4} p_{CO_2} + K_1 k_2 p_{CH_4} + k_3 p_{CO_2}} \times \frac{K_{DRM} p_{CH_4} p_{CO_2} - (p_{CO} p_{H_2})^2}{K_{DRM} p_{CH_4} p_{CO_2}}$ **Numerator:** 1.94e−2 × exp(4550/T) × 419.4 × exp(−11111/T) × 102.3 × exp(−231.6/T) × R_1 × R_2 × (6.78e+14 × exp(−31232/T) × R_1 × R_2−(P_1 × P$_2$)^2) **Denominator:** 1.94e−2 × exp(4550/T) × 102.3 × exp(−231.6/T) × R_1 × R_2 + 1.94e−2 × exp(4550/T) × 419.4 × exp(−11111/T) × R_1 + 102.3 × exp(−231.6/T) × R_2 × (6.78e+14 × exp(−31232/T) × R_1 × R_2)	Eq. (4) × Eq. (10)
$r_{CH_4} = \frac{K_1 k_2 k_3 p_{CH_4} p_{CO_2}}{K_1 k_3 p_{CH_4} p_{CO_2} + K_1 k_2 p_{CH_4} + k_3 p_{CO_2}} \times \frac{K_{DRM} p_{CH_4} p_{CO_2} - (p_{CO} p_{H_2})^2}{K_{DRM} p_{CH_4} p_{CO_2}}$ **Numerator:** 1.46e−4 × exp(7242/T) × 2.94e+3 × exp(−12949/T) × 4.05e+10 × exp(15891/T) × R_1 × R_2 × (6.78e+14 × exp(−31232/T) × R_1 × R_2−(P_1 × P_2)^2) **Denominator:** 1.46e−4 × exp(7242/T) × 4.05e+10 × exp(15891/T) × R_1 × R_2 + 1.46e−4 × exp(7242/T) × 2.94e+3 × exp(−12949/T) × R_1 + 4.05e+10 × exp(15891/T) × R_2 × (6.78e+14 × exp(−31232/T) × R_1 × R_2)	Eq. (5) × Eq. (10)

Table A1 DRM and RWGS kinetic rate model input in DWSIM (continued)

$$r_{CH_4} = \frac{k_1\ p_{CH_4}\ p_{CO_2}}{k_2\ p_{CH_4} + k_3\ p_{CO_2}} \times \frac{K_{DRM}\ p_{CH_4}\ p_{CO_2} - \left(p_{CO}\ p_{H_2}\right)^2}{K_{DRM}\ p_{CH_4}\ p_{CO_2}}$$	Eq. (6) × Eq. (10)
Numerator: 1.35e−4 × exp(−25900/8.314/T) × R_1 × R_2 × (6.78e+14 × exp(−31232/T) × R_1 × R_2−(P_1 × P_2)^2) **Denominator:** 9.25e−6 × exp(40600/8.314/T) × R_1 + 2.46e−5 × exp(38300/8.314/T) × R_2 × (6.78e+14 × exp(−31232/T) × R_1 × R_2)	
$$r_{CH_4} = \frac{K_1\ k_2\ k_3\ p_{CH_4}\ p_{CO_2}}{K_1\ k_3\ p_{CH_4}\ p_{CO_2} + K_1\ k_2\ p_{CH_4} + k_3\ p_{CO_2}} \times \frac{K_{DRM}\ p_{CH_4}\ p_{CO_2} - \left(p_{CO}\ p_{H_2}\right)^2}{K_{DRM}\ p_{CH_4}\ p_{CO_2}}$$	
Numerator: 2.9755e+4 × exp(−7502.5/T) × 12.27 × exp(−10219.2/T) × 3.4 × exp(−4990/T) × R_1 × R_2 × (6.78e+14 × exp(−31232/T) × R_1 × R_2−(P_1 × P_2)^2) **Denominator:** 2.9755e+4 × exp(−7502.5/T) × 3.4 × exp(−4990/T) × R_1 × R_2 + 2.9755e+4 × exp(−7502.5/T) × 12.27 × exp(−10219.2/T) × R_1 + 3.4 × exp(−4990/T) × R_2 × (6.78e+14 × exp(−31232/T) × R_1 × R_2)	Eq. (7) × Eq. (10)
$$r_{CH_4} = \frac{K_1\ k_2\ K_3\ k_4\ p_{CH_4}\ p_{CO_2}}{K_3\ k_4\ p_{CO_2} + K_1\ K_3\ k_4\ p_{CH_4}\ p_{CO_2} + K_1\ k_2\ p_{CH_4} + K_1\ k_2\ K_3\ p_{CO_2}} \times \frac{K_{DRM}\ p_{CH_4}\ p_{CO_2} - \left(p_{CO}\ p_{H_2}\right)^2}{K_{DRM}\ p_{CH_4}\ p_{CO_2}}$$	
Numerator: 7.82e−4 × exp(8280/T) × 48000 × exp(−16470/T) × 7.54e−5 × exp(9200/T) × 632 × exp(−12110/T) × R_1 × R_2 × (6.78e+14 × exp(−31232/T) × R_1 × R_2−(P_1 × P_2)^2) **Denominator:** 7.54e−5 × exp(9200/T) × 632 × exp(−12110/T) × R_2 + 7.82e−4 × exp(8280/T) × 7.54e−5 × exp(9200/T) × 632 × exp(−12110/T) × R_1 × R_2 + 7.82e−4 × exp(8280/T) × 48000 × exp(−16470/T) × R_1 + 7.82e−4 × exp(8280/T) × 48000 × exp(−16470/T) × 7.54e−5 × exp(9200/T) × R_2 × (6.78e+14 × exp(−31232/T) × R_1 × R_2)	Eq. (8) × Eq. (10)
RWGS kinetic rate model	
$$r_{CO_2} = \frac{k_1\ K_2\ K_3\ p_{CO_2}\ p_{H_2}}{\left(1 + K_2\ p_{CO_2} + K_3\ p_{H_2}\right)^2} \left(\frac{K_{RWGS}\ p_{CO_2}\ p_{H_2} - p_{H_2O}\ p_{CO}}{K_{RWGS}\ p_{CO_2}\ p_{H_2}} \right)$$	Eq. (9)
Numerator: 350 × exp(−9746/T) × 0.5771 × exp(1114/T) × 1.494 × exp(724.7/T) × R_1 × R_2 × (56.4971 × exp(−4340/T) × R_1 × R_2−P_1 × P_2) **Denominator:** ((1+0.5771 × exp(1114/T) × R_1 + 1.494 × exp(724.7/T) × R_2)^2) × 56.4971 × exp(−4340/T) × R_1 × R_2	